Revealing the powdering methods of black makeup in Ancient Egypt by fitting microstructure based Fourier coefficients to the whole x-ray diffraction profiles of galena

T. Ungár, P. Martinetto, G. Ribárik, E. Dooryhée, Ph. Walter, and M. Anne

Citation: Journal of Applied Physics **91**, 2455 (2002); doi: 10.1063/1.1429792
View online: http://dx.doi.org/10.1063/1.1429792
View Table of Contents: http://scitation.aip.org/content/aip/journal/jap/91/4?ver=pdfcov
Published by the AIP Publishing

Revealing the powdering methods of black makeup in Ancient Egypt by fitting microstructure based Fourier coefficients to the whole x-ray diffraction profiles of galena

T. Ungár[a)]
Department of General Physics, Eötvös University Budapest, P.O. Box 32, H-1518, Budapest, Hungary

P. Martinetto
Centre de Recherche et de Restauration des Musées de France, 6 rue des Pyramides, 75041 Paris cedex 1, France

G. Ribárik
Department of General Physics, Eötvös University Budapest, P.O. Box 32, H-1518, Budapest, Hungary

E. Dooryhée
Laboratoire de Cristallographie-CNRS, 25 avenue des Martyrs, BP 166, 38042 Grenoble cedex 9, France

Ph. Walter
Centre de Recherche et de Restauration des Musées de France, 6 rue des Pyramides, 75041 Paris cedex 1, France

M. Anne
Laboratoire de Cristallographie-CNRS, 25 avenue des Martyrs, BP 166, 38042 Grenoble cedex, 9, France

(Received 30 April 2001; accepted for publication 29 October 2001)

Galena (PbS) is a major ingredient in ancient Egyptian eye makeup. The microstructure of PbS in Egyptian cosmetic powders is used as a fingerprint and is matched with the microstructures produced artificially in geological galena minerals. The microstructure of PbS is determined by x-ray diffraction peak profile analysis in terms of dislocation density, crystallite size, and size distribution. High-resolution powder diffractograms were measured at the ESRF Grenoble synchrotron source with high resolution and high peak-to-background ratios. The Fourier coefficients of the first nine measured reflections of galena are fitted using physically based Fourier coefficients of strain and size functions. Strain anisotropy is accounted for by the dislocation model of the mean square strain. The x-ray data are supplemented by scanning electron microscopy (SEM) and transmission electron microscopy (TEM) micrographs, and are compared with archæological documents. It enables us to describe the procedures of eye makeup manufacturing in the Middle and New Kingdoms of Egypt some 2000 years before Christ. © *2002 American Institute of Physics.* [DOI: 10.1063/1.1429792]

I. INTRODUCTION

A. The archæological background

It is well known that makeup, unguents, and tattoos have been extensively used since the very early times of humanity. Egyptian civilization in particular gives us a chance to determine the origins, the methods, and the goals of the cosmetic industry in the Antiquity. A variety of containers (stone vases, reeds, or wooden receptacles) full of makeup is often present in the burial furniture of Egypt dated between 2000 and 1200 B. C.; their abundance and manufacture show how important the cosmetics were in the social and religious practices of everyday life, as well as in the deceased's afterlife.[1–5] We have examined the mineral content of as many as 52 different toilet accessories, preserved in an exceptionally good state at the Louvre Museum.[6] Up to 75% of the analyzed powders are mixtures of lead compounds. Two well-known natural lead-based compounds are identified: the black ore of galena (PbS) and the white cerussite ($PbCO_3$).[7] Unexpectedly, our analyses also reveal the adjunction of two more white lead derivatives obtained by wet chemistry: laurionite (PbOHCl) and phosgenite ($Pb_2Cl_2CO_3$).[7] It is well established that later during the Roman period, these synthetic compounds were employed as pharmaceutical products to treat some eye illnesses.[8,9] Some medical papyri of the pharaohs' period also mention that the makeup could alternatively be used as a sort of lotion for eye care.[10]

The substances present in the makeup are highly crystalline and can be readily identified and weighed by the means of x-ray and neutron powder diffractometry. Due to the scarcity and the high absorbence of these lead substances, the high energy and the high flux of synchrotron radiation are particularly well suited for their analysis. Thanks to the high resolution of the synchrotron diffractograms, one can separate out overlapping reflection peaks originating from different constituent phases; in addition, the reflection peak profile can be rationalized in terms of both size distribution and type, and average magnitude of the lattice internal strain of

a)Electronic mail: ungar@ludens.elte.hu

the crystallites composing the powder. The microstructure parameters (size and strain) of the main ingredient phases give some key information as to the preparation of the lead minerals, whether the cosmetic powders were either synthesized or crushed, sieved or possibly annealed at low temperatures before being incorporated into the makeup. The scanning electron micrographs show that the galena phase is made of ~5–100 μm grains, which were extracted out of the ore gangue by hand milling, and sorted out by size in order to control the texture and brightness of the powder. Conversely, laurionite was synthesised in solution and the powder granulometry is markedly different. The average microstructure of the crystallites can be determined nondestructively by the analysis of the shape of the diffraction peaks, and is the signature of these different manufacturing processes.

B. Principles of diffraction peak profile analysis

Particle or crystallite size, such lattice defects as dislocations, stacking faults, grain boundaries, inclusions, precipitates, etc., are the constituents of the microstructure in crystalline materials. One of the most straightforward methods to visualize the microstructure is transmission electron microscopy. It provides the local details; however, it is difficult to obtain some statistically representative information over large volumes and/or in a great number of specimens. A complementary tool for studying the microstructure is x-ray diffraction peak profile analysis. It has the advantage of giving information about averages over larger volumes and is sensitive to the strain fields of lattice defects, especially the different internal stresses related to dislocations. In the present work it is shown that the appropriate combination of the theoretically correct size[11,12,13] and strain[14] profiles makes it possible to describe the whole powder diffraction profiles with physically based functions.[15,16]

Two classical procedures emerged in the past to separate size and strain broadening: the Williamson–Hall[17] and the Warren–Averbach methods.[18,19] The first cannot deal properly with strain anisotropy. The second, in addition to that restriction, cannot deal properly with the mean square strain. The dislocation models of strain anisotropy[20,21] and of the mean square strain[14,22] enabled us to rehabilitate both methods: they are referred to as the *modified* Williamson–Hall and the *modified* Warren–Averbach methods.[20] They were successfully applied to characterize the microstructure of plastically deformed metals[20,23–25] or ionic crystals[26–28] in terms of crystallite size and dislocation densities. Further development and improvement of the *modified* methods have been achieved by using physically based functions for both the size and the strain profiles, and taking into account strain anisotropy by means of the dislocation contrast factors.[15,16] A procedure has been developed for fitting the microstructure based, physically correct Fourier coefficients to the whole powder diffraction profiles.[15,16] In the case of cubic crystals, five parameters are used: the median and the width of a log-normal size distribution function (m and σ, respectively), the densities and the effective outer cutoff radius of dislocations (ρ and R_e, respectively), and the q parameter for the average dislocation contrast factors. The procedure is applied to geological and archæological galena, in which the geological specimens were prepared into different states by ball-milling, sieving, and/or annealing.

II. MULTIPLE WHOLE PROFILE FITTING USING THE FOURIER COEFFICIENTS OF PHYSICALLY BASED FUNCTIONS

In the kinematical theory of x-ray diffraction, the physical profile of a Bragg reflection I^F is equal to the convolution of the size and distortion (or strain) profiles, I^S and I^D:[11,19]

$$I^F = I^S * I^D. \tag{1}$$

The Fourier transform of this equation is known as the Warren–Averbach equation:[18,19]

$$A_L^F(g) = A_L^S \exp[-2\pi^2 L^2 g^2 \langle \epsilon_{g,L}{}^2 \rangle], \tag{2}$$

where $A_L^F(g)$ are the moduli of the Fourier coefficients of the physical profiles, A_L^S are the size Fourier coefficients, and the strain Fourier coefficients are the exponential expression of Eq. (2). g is the absolute value of the diffraction vector, and $\langle \epsilon_{g,L}{}^2 \rangle$ is the mean square strain in the g direction. L is the Fourier length defined as $L = na_3$,[18] where $a_3 = \lambda/2(\sin\theta_2 - \sin\theta_1)$, n are integers starting from zero, λ is the wavelength of x-rays, and $(\theta_2 - \theta_1)$ is the angular range of the measured diffraction profiles. The entire expression on the right-hand side of Eq. (2) can be evaluated over the whole L range on a physically sound basis.[11–16] A brief summary is given here.

A. The Fourier coefficients of the size profile

Assuming the most commonly observed log-normal size distribution function[29,30] and spherical crystallites, the size Fourier coefficients can be given as[15,16]

$$A^S(L) \sim \frac{m^3 \exp(4.5\sigma^2)}{3} \operatorname{erfc}\left[\frac{\log(|L|/m)}{\sqrt{2}\sigma} - 1.5\sqrt{2}\sigma\right] - \frac{m^2 \exp(2\sigma^2)|L|}{2} \operatorname{erfc}\left[\frac{\log(|L|/m)}{\sqrt{2}\sigma} - \sqrt{2}\sigma\right] + \frac{|L|^3}{6} \operatorname{erfc}\left[\frac{\log(|L|/m)}{\sqrt{2}\sigma}\right], \tag{3}$$

where x is the grain or crystallite size, σ and m are the variance and the median of the size distribution function, respectively, and erfc is the complementary error function. In principle, the as-obtained Fourier transform of the form function of the crystallites can be computed for any crystallite shape and any size distribution.[15] Hinds has shown that the area, volume, and arithmetically weighted mean crystallite sizes can be obtained from m and σ in a straightforward manner:[31]

$$\langle x \rangle_{\text{area}} = m \exp(2.5\sigma^2), \tag{4}$$

$$\langle x \rangle_{\text{vol}} = m \exp(3.5\sigma^2), \tag{5}$$

and

$$\langle x \rangle_{\text{arithm}} = m \exp(0.5\sigma^2). \tag{6}$$

Size broadening is caused by the column length of coherently scattering domains parallel to the diffraction vector. Coherently scattering domain means the region wherein the amplitudes of the scattered x rays sum up. When the crystallographic orientation between regions exceeds a few degrees, the amplitude summation ends and intensities are summed up.[11] It is important to note that single dislocations do not disturb the coherency of x-ray scattering, since the misorientation they cause is of the order of $b\rho^{1/2}$, where b and ρ are the Burgers vector and density of dislocations, respectively. Typical values in galena are 0.36 nm and 5×10^{14} m^{-2}, giving misorientations of the order of $\sim0.4°$. On the other hand, special arrays or bundles of dislocations can easily create misorientations of a few degrees, thus creating boundaries of the coherently scattering regions. There may be some sort of proportionality between the x-ray crystallite size and the grain or particle size determined by SEM or TEM. However, to the best knowledge of the authors this has not yet been studied, and goes beyond the scope of this work. From this we concluded that: (i) the dislocation density (or microstrain) is a microstructural parameter independent of crystallite size (domain size) and that neither can be deduced from the other, and (ii) the x-ray crystallite size can never be larger than the grain or particle size obtained by SEM or TEM.

B. The dislocation model of the mean square strain

Based on the classification of lattice by Krivoglaz,[22] it can be shown that dislocations or dislocationlike lattice defects play the most important role in strain broadening. Lattice defects can be categorized according to the spatial dependence of the distortion $\epsilon(r)$: (i) planar faults, such as stacking faults or grain boundaries, (ii) dislocations or dislocationlike defects, and (iii) point defects: vacancies, interstitials, small precipitates, or small inclusions. The spatial dependence of ϵ is: (i) $\sim$constant, (ii) $\sim1/r$, and (iii) $\sim1/r^2$, respectively. When $\epsilon(r)$ is constant the diffraction profiles are mainly shifted, as is the case for stacking faults and/or grain boundaries.[19,32] When $\epsilon(r)$ is proportional to $1/r^2$ the distortion is of short-range character, and the diffraction effects are manifested in the regions far from the fundamental Bragg reflections, as in Huang scattering.[33] Those distortions which affect the regions close to the fundamental Bragg reflections have to be of long-range character and typically are dislocations. For this reason, in the present work, strain broadening will be attributed to dislocations.

Krivoglaz,[22] Wilkens[14] and others[34–38] have shown that the mean square strain for dislocations can be expanded into a logarithmic series in which the leading term is

$$\langle \epsilon_{g,L}{}^2\rangle \cong \frac{\rho C b^2}{4\pi}\log(R_e/L), \tag{7}$$

where ρ is the density, R_e the effective outer cutoff radius, b the Burgers vector, and C the contrast factor of dislocations. The only *hkl*-dependent term on the right hand side is the contrast factor C. Eq. (7) is valid only for small L values, in particular for $L<R_e$. Wilkens evaluated $\langle \epsilon_{g,L}{}^2\rangle$ in the entire range of L for screw dislocations.[14] Since this is probably the best available expression of $\langle \epsilon_{g,L}{}^2\rangle$ for dislocations, we are going to use it as the *physically based* function for strain broadening. Kamminga and Delhez have recently found that the expressions derived by Wilkens for screw dislocations are also valid for edge dislocations.[38] The detailed expression of $\langle \epsilon_{g,L}{}^2\rangle$ given by Wilkens can be found in Eqs. A.6 to A.8 in Ref. 14 and in Eqs. (22) and (23) in Ref. 15. It has the following structure:

$$\langle \epsilon_{g,L}{}^2\rangle = (b/2\pi)^2\pi\rho C f(\eta), \tag{8}$$

where $\eta\cong L/R_e$. In the following, $f(\eta)$ is called the Wilkens function. Instead of R_e, it is physically more appropriate to use the dimensionless parameter $M=R_e\sqrt{\rho}$, defined by Wilkens as the dislocation arrangement parameter.[14] The value of M gives the strength of the dipole character of dislocations: if M is small (or large) the dipole character and the screening of the dislocation strain fields is strong (or weak, respectively). At the same time, strong (or weak) screening and small (or large) values of M means strong (or weak) correlations in the dislocation distributions and long (or short) tails in the diffraction profiles.

C. The contrast factors of dislocations

A great deal of experimental evidence has shown that strain broadening is anisotropic.[39–43] This means that neither the full width at half maximum (FWHM), nor the integral breadth in the Williamson–Hall plot, nor the Fourier coefficients in the Warren–Averbach plot are monotonous functions of the diffraction vector or its square, g or g^2, respectively. Phenomenological models based on the elastic anisotropy of crystals have been suggested and have proved to be successful.[43,44] However a more fundamental model can describe strain anisotropy on the basis of the anisotropic contrast effect of dislocations.[20,21,23–28,32,45] The strength of peak broadening caused by dislocations depends on the relative orientations between the Burgers- and the line vectors of dislocations, and the diffraction vector, b, l, and g, respectively, and the elastic constants of the material. This is accounted for by the contrast factors $C=C(b,l,g,c_{ij})$, as indicated in Eqs. (7) and (8), where $c_{i,j}$ are the elastic constants of the crystal. If the specimen is a powder, the contrast factors can be averaged over the permutations of *hkl* for each reflection. In a recent work it has been shown that these average contrast factors are a simple function of *hkl*,[21] in particular, for cubic crystals:

$$\overline{C}=\overline{C}_{h00}(1-qH^2), \tag{9}$$

where $\overline{C}_{h00}$ is the average contrast factor for the $h00$ reflections, q is a parameter depending on the elastic constants of the crystal and on the edge or screw character of dislocations, and $H^2=(h^2k^2+h^2l^2+k^2l^2)/(h^2+k^2+l^2)^2$.

D. The fitting procedure

A numerical procedure has been worked out for fitting the Fourier coefficients of the experimentally determined physical profiles by the Fourier coefficients of the theoretical size and strain functions using Eq. (2).[16] The measured profiles must first be corrected for background, instrumental effects, and overlapping peaks. The numerical procedure fol-

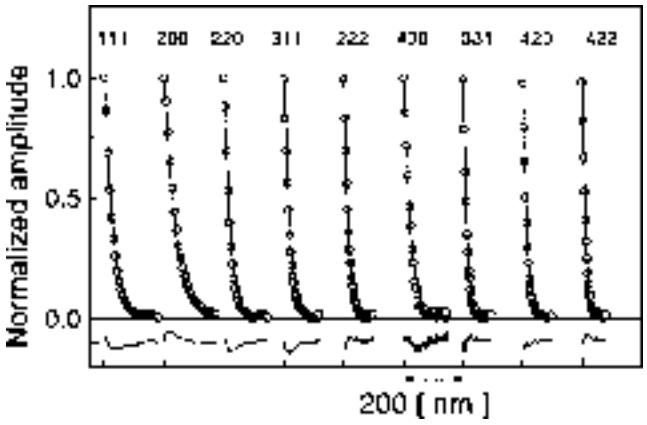

FIG. 1. A typical example of the fitting of the Fourier coefficients of the measured physical profiles (open circles) by the theoretical Fourier transforms (solid lines) for the *U_60_25* specimen (geological material ball-milled for 1 h). The differences between the fitted and measured Fourier coefficients are indicated at the bottom of the figure.

lows the following steps: (i) Fourier coefficients of the measured physical profiles are computed using the Stokes method, (ii) Fourier coefficients of the theoretical size and strain profiles are calculated using Eqs. (3) and Eqs. A.6–A.8 in Ref. 14 and/or Eqs. (22) and (23) in Refs. 15, and Eq. (9), and (iii) the calculated Fourier coefficients are fitted to the experimental values using the nonlinear Marquardt–Levenberg least-squares procedure (GNUPLOT program package under UNIX). For more details of the numerical procedure see Ref. 16. The following five fitting parameters are used: m and σ, the median and the variance of the log-normal size distribution function for the size profile, respectively; ρ and M, the density and the arrangement parameter of dislocations for the strain profile, respectively; and q, the average dislocation contrast factors as in Eq. (9). The value of $\overline{C}_{h00}$ is not a fitting parameter since it is only a multiplicative factor in the Fourier coefficients of the strain profiles. The value of q has been obtained as: $q=-6.5\pm1$ for all the galena specimens investigated here. The elastic constants of PbS have recently been determined by Kim and Ledbetter.[46] They found that the elastic anisotropy or the Zener constant of PbS is $A_z=0.311$, which is in excellent correlation with the q parameter value determined experimentally here (see also Fig. 2 in Ref. 45 and Fig. 2 in Ref. 47). Assuming equal populations of edge and screw dislocations, $\overline{C}_{h00}=0.12\pm0.02$.[45,47] Figure 1 shows a typical example of the fitting of the Fourier coefficients of the measured physical profiles (open circles) by the theoretical Fourier transforms given in Eq. (2), Eqs. (22) and (23) in Ref. 15, and Eq. (9) (solid lines) for the *U_60_25* specimen (geological material ball-milled for 1 h at room temperature). The differences between the fitted and measured Fourier coefficients are also indicated at the bottom of Fig. 1. The inverse Fourier transforms of the theoretical and measured Fourier coefficients corresponding to the same nine diffraction peaks were usually also in excellent correlation with each other. The fitting procedure is worked out in Fourier space, owing to the fact that the microstructure based and physically correct strain profile given by the Wilkens function $f(\eta)$ is expressed in the Fourier space. A numerical procedure operating directly on the measured profiles in the 2θ space and using the $f(\eta)$ function would probably need unforeseeable computational time and therefore has not yet been attempted; however, it would be desirable.

III. EXPERIMENTAL PROCEDURES

A. Specimens

The size distribution and the strain were measured in a large number of geological PbS powders as a function of the applied treatment (crushing, annealing, sieving). These simulations on geological materials were used to consolidate our data reduction method and our model, and to interpret the microstructure of the as-found archæological powders. Three independent batches of PbS powders from different mining sources (France, Egypt, and North America) were compared. They are named F (France), E (Egypt), and U (North America). The as-received ores were hand-milled and sieved with a grid mesh of 63–125 μm size. Subsequently, the geological galena minerals were either annealed for 2 h in capillaries sealed under vacuum, or crushed in a planetary ball milling device, or both. The annealing temperatures range between 100 and 800 °C. The mechanical grinding duration time varies between 10 min and 12 h. The specimen name is coded as *X_t_T*, where *X* refers to the mining origin of galena (*U*, *F*, or *E*), *t* is the grinding time in minutes in an automatic device using spinning agate balls, and *T* is the annealing temperature in °C for 2 h in capillaries sealed under vacuum. *Ufin* is the fraction made of fine grains which passed through the 63–125 μm grid mesh (in the following this notation will be used for this fraction), whereas *U_0_25* is the complementary residual fraction made of larger crystallites. *U_10_25* is obtained from sample *U_0_25* after 10 min mechanical ball milling. *U_120_100* is sample *U_0_25* after 2 h milling and 2 h annealing at 100 °C. *U_720_300* is sample *U_0_25* after 12 h milling and 2 h annealing at 300 °C.

Archæological PbS was extracted from eight different galena-rich cosmetic powders of the Middle and New Kingdoms. Their code numbers from the department of the Egyptian Antiquities of Le Louvre Museum are: *E11047*, *E14455*, *E23100*, *E21562*, *E23105*, *N811d*, *N811g*, and *N1332*. Table I gives the mass fractions of the major phases in these specimens, as obtained from x-ray diffraction quantitative analysis using the Rietveld pattern refinement method.[48]

B. Synchrotron measurements

The archæological and geological PbS powders were individually packed into 0.4 mm glass capillaries and mounted in the Debye–Scherrer mode on the ESRF-BM 16 high-resolution diffractometer.[49] The 2θ arm of the diffractometer is equipped with nine parallel pairs of analyzer crystals and photon scintillation counters, and scans continuously around the capillary. Using a third-generation source for parallel beam optics (very low vertical divergence of the incident x ray beam), the diffraction peak shape is critically sensitive to the number and to the orientation averaging of the probed

TABLE I. Quantitative analysis of the archæological powders, mass fractions of the five major lead constituents.

Sample	Datation	Galena	Anglesite	Cerussite	Phosgenite	Laurionite
*E*11047	New Kingdom	41		41	18	
*E*14455	New Kingdom	70	10	*+zinc-based phases (20%)*		
*E*21562	Middle or New Kingdom	15	9	25	32	19
*E*23100	Middle Kingdom	58	19	19		4
*E*23105	Middle Kingdom	44		+ quartz(38%) + calcite(18%)		
*N*811*d*	New Kingdom	75		14	11	
*N*811*g*	New Kingdom	75		14	11	
*N*1332	New Kingdom	89		4	5	2

crystallites in the powder. That makes it necessary to spin the capillary at ~100 rpm about the goniometer axis. The normal diffraction pattern is recomposed after binning the individual detector counts in $0.002° 2\theta$ steps, summing over the nine channels and normalizing against the incident beam intensity. The diffraction peaks of the compound $Na_2Ca_3Al_2F_{14}$ were measured over the 2θ angular region of interest, in the same conditions as the geological and archæological specimens.[50] The crystallites of $Na_2Ca_3Al_2F_{14}$ are sufficiently large and free of any lattice distortion; therefore the Bragg reflection profiles of $Na_2Ca_3Al_2F_{14}$ are immune to any sample broadening effect.[51] The wavelength was calibrated as $\lambda = 0.0445$ nm by measuring the 2θ peak positions of NBS NIST SRM640 silicon.

The measured FWHM of the diffraction peaks of the as-received galena specimen (*U_0_25*) are plotted as a function of the scattering vector (open squares) and compared with (i) the instrumental breadths of the high-resolution powder diffractometer at the beamline BM16 of the synchrotron ESRF in Grenoble, France, measured with the $Na_2Ca_3A_{12}F_{14}$ reference compound (bottom solid line) and (ii) the instrumental breadths of the Bruker D5000 laboratory diffractometer (upper solid line) in Fig. 2. The figure shows that the peak breadths of galena can be relatively small (i.e., $\leqslant 0.01° 2\theta$). For this reason the correct separation of sample broadening and instrumental broadening could not be done reliably with laboratory data. The deconvolution was possible with the data collected at BM16, where the instrumental contribution into the peak breadth can be as small as $0.003° 2\theta$.

C. Preparation of the diffraction data for the fitting procedure

For the purpose of (i) the elimination of small parasitic peaks due to minority phases, especially in the case of the archæological specimens, (ii) the separation of overlapping peaks, typically in the case of the 311 and 222 reflections, and (iii) subtraction of a linear or quadratic polynomial background, an auxiliary peak fitting program was used. The program enables a number of the most common peak functions; however, in the present case the pseudo-Voigt or Pearson VII functions were used most successfully. After subtraction of the appropriate background and removal of any possible unwanted parasitic or overlapping peaks, the measured and thus corrected datapoints were used in the evaluation procedure. For further details of the data correction procedure see Ref. 16. It is important to stress here that the simple peak functions, as pseudo-Voigt or Pearson VII, were used only for removing neighboring extra peaks and background. All further evaluation was carried out (a) on the measured (background removed) datapoints and (b) by using the physical functions and procedures described above. For removing the instrumental effects on the peak shape, each sample diffraction peak and the closest diffraction peak of the reference $Na_2Ca_3Al_2F_{14}$ compound were independently measured. Since the $Na_2Ca_3Al_2F_{14}$ specimen has a large number of reflections distributed relatively equally over the entire diffraction range, the angular distance between the measured sample peak and the closest instrumental peak was never

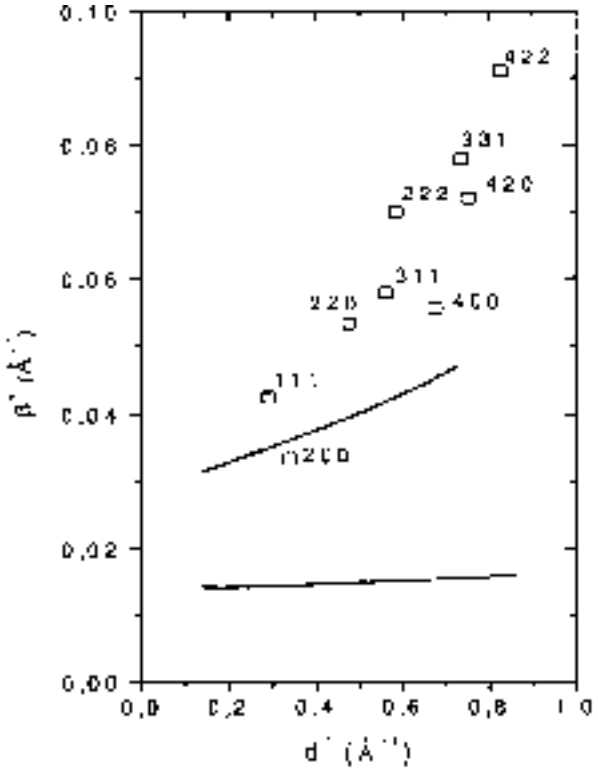

FIG. 2. Williamson–Hall graph: the observed FWHM of the diffraction peaks of galena (*U_0_25*) are plotted (squares) in the reciprocal space as a function of the scattering vector, and compared with the instrumental breadths (measured with the $Na_2Ca_3Al_2F_{14}$ reference compound) of BM 16 (bottom solid line) and of Bruker D 5000 laboratory diffractometer (upper solid line).

TABLE II. The average dislocation densities ρ, the variance σ, and the median m, of the crystallite size distribution functions [see Eq. (3)], the volume average crystallite diameter, $\langle x\rangle_{\rm vol}$ (this method), the apparent crystallite size corresponding to the Fourier coefficients L_0, and the mean square strain $\langle \epsilon^2\rangle$, as obtained by the *modified* Warren–Averbach method, for the geological specimens.

Sample treatment	Temperature (°C)	ρ (10^{14} m^{-2})	σ	m (nm)	$\langle x\rangle_{\rm vol}$ (nm)	L_0 (nm)	$\langle \epsilon^2\rangle \times 10^5$
U, uncrushed	RT[a]	3.3 (0.5)	0.67	99	490	151	15
	100	2.1 (0.5)	0.80	62	580	145	8.7
	200	0.6 (0.2)	0.51	242	600	183	7.2
	300	0.28 (0.1)	0.74	197	1400	371	5.5
	500	0.38 (0.1)	0.01	1404	1400	526	3.5
	800	0.15 (0.1)	0.45	1090	2200	1230	3.1
U, 10 min	RT	7.3 (1)	0.85	25	320	108	33.7
crushing	100	8 (1)	0.84	26	300	109	31.5
	300	2 (0.5)	0.59	143	480	231	19.3
	500	0.3 (0.1)	0.78	124	1040	296	4.7
U, 1 h crushing	RT	12 (1)	0.73	21	130	45	45
	100	9.7 (1)	0.68	27	140	52	45
	300	3.5 (1)	0.63	53	210	96	26.2
U, 2 h crushing	RT	14.1 (1)	0.86	14	185	71	48.2
	100	5.9 (1)	0.60	49	175	72	42.5
	200	6.4 (1)	0.61	46	170	76	39.1
	300	2.6 (0.5)	0.56	96	290	118	19.1
	400	1.3 (0.5)	0.67	84	400	260	7.4
	500	0.4 (0.1)	1.14	20	2000	900	2.4
U, 12 h	RT	39 (5)	0.81	7.6	80	25	72
crushing	300	8.2 (1)	0.54	62	170	92	28.5
	500	1 (0.5)	0.86	42	560	159	8
E, uncrushed	RT	7 (2)	0.75	86	630	142	11.2
E, 2 h crushing	RT	9 (2)	0.76	22	160	73	49
F, uncrushed	RT	3 (2)	0.8	62	560	133	10.5
F, 2 h crushing	RT	10 (5)	0.72	32	200	77	42.8
Ufin (fine sieving)	RT	4.7	0.85	25	350	110	26.2

[a]Room temperature.

larger than $\Delta(2\theta)=1°$. Both the observed (sample, uncorrected) and the reference ($Na_2Ca_3Al_2F_{14}$, instrument) profiles are Fourier transformed. The discrete Fourier transformation was applied numerically on each individual raw profile, as obtained after removal of background and overlapping peaks. The discrete Fourier coefficients A of the physical profiles are obtained from the normal Stokes procedure.[52]

IV. RESULTS

In order to identify the physical aspects of the manufacturing procedures of the archæological powders, crushing and heating were carried out on the PbS specimens obtained from French, North American, and Egyptian natural sources. The volume average crystallite diameters, the average dislocation densities, the median and the variance of the size distribution function, $\langle x\rangle_{\rm vol}$, ρ, m, and σ, respectively, provided by the method described here, are listed in Table II. The same parameters corresponding to the eight investigated archæological specimens are given in Table III. The data are between brackets when: (i) $\langle X\rangle_{\rm vol}$ is too large and out of the resolution range of detectable size broadening (larger than about a micron) or (ii) the determination of the dislocation density has not been successful. The last two columns in Tables II and III are the L_0 and $\langle \epsilon^2\rangle$ determined from the *modified* Warren–Averbach procedure.[20]

A. Comparison with the modified Warren–Averbach method

The nonmonotonous variation of the *hkl* breadths of galena in the Williamson–Hall graph of Fig. 2 is caused mainly by strain anisotropy. It can be eliminated by introducing the average dislocation contrast factors according to the dislocation model of the mean square strain.[20,21] The average contrast factor has been calculated with $q=-6.5$, in agreement with Sec. II D. In such a case the reflections with indices $h00$ are the narrowest peaks. In the resulting *modified* Warren–Averbach[20] graph shown in Fig. 3, the absolute logarithmic values of the normalized Fourier coefficients $A(L)$ are plotted versus $K^2\overline{C}$. The rearranged sequence of the diffraction peaks can be seen by the indices listed in the top of the figure, in the case of the as-received geological specimen *U_0_25*. The quadratic functions fitted to the data points are indicated as solid lines in a few cases. The intercepts at $K=0$ give the size Fourier coefficients $A^S(L)$, and the initial slope yields the strain Fourier coefficients $A^D(L)$. From the $A^S(L)$ versus L plot, the area weighted apparent

TABLE III. The average dislocation densities ρ, the variance σ, and the median m, of the crystallite size distribution functions [see Eq. (3)], the volume average crystallite diameter, $\langle x\rangle_{\rm vol}$, (this method), the apparent crystallite size corresponding to the Fourier coefficients L_0, and the mean square strain $\langle\epsilon^2\rangle$, as obtained by the *modified* Warren–Averbach method, for the archæological specimens.

Name of specimen	ρ (10^{14} m^{-2})	σ	m (nm)	$\langle x\rangle_{\rm vol}$ (nm)	L_0 (nm)	$\langle\epsilon^2\rangle$ ($\times 10^5$)
*E*14455	2.4	0.73	75.6	517	153	18
*E*21562	1.2	0.28	295.4	385	-	-
*E*23100	2.7	0.44	225.7	446	238	17
*E*23105	1.1	0.58	138.9	452	180	17
*E*11047	5.4	0.71	36.2	210	62	55
*N*1332	5.9	0.46	113.9	236	116	34
*N*811*d*	10.3	0.68	25.6	131	78	34
*N*811*g*	8.8	0.87	15.7	218	74	44

size parameter L_0 is obtained. $L_0=150\pm15$ nm for *U_0_25*. Using the m and σ values of specimen *U_0_25* from Table II and using Eq. (4), $\langle X\rangle_{\rm area}=304\pm15$ nm is obtained. Taking into account that $\langle X\rangle_{\rm area}\sim(3/2)L_0$ (see Ref. 31), the value of the apparent size L_0 obtained by the *modified* Warren–Averbach method is by about 25% smaller than the area weighted average crystallite diameter $\langle X\rangle_{\rm area}$ provided by the profile fitting procedure. This small discrepancy is most probably due to the fact that in the *modified* Warren–Averbach method, only those Fourier coefficients are taken into account in the strain evaluation for which $L\leqslant R_e$. This condition might put slightly different weights on size and strain contributions as compared to the weights in the profile fitting procedure. We note, however, that the $\langle X\rangle_{\rm area}$ values calculated from m and σ (see in Table II and III) are highly correlated at $\pm10\%$ with L_0 in the geological samples. Only the most severely annealed samples or uncrushed samples, that contain large crystallites, i.e., $L_0>120$ nm, show some disagreement. For the sake of correspondence with more classical evaluation and interpretation methods, a particular mean square strain value, $\langle\epsilon^2\rangle_{L=0.5\,\rm nm}$, corresponding to $L=0.5$ nm has also been determined from the $A^D(L)$ versus L plot, and these values are listed in Tables II and III. The $\langle\epsilon^2\rangle_{L=0.5\,nm}$ and ρ values are in correlation at $\pm35\%$ in geological galena, except when the powder has been severely crushed or when the deconvolution into size and strain has been questionable.

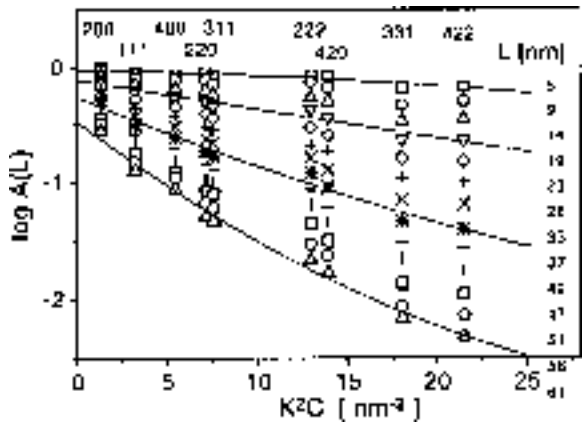

FIG. 3. A typical *modified* Warren–Averbach plot of the absolute logarithmic values of the normalized Fourier coefficients $A(L)$ plotted vs $K^2\overline{C}$, in the case of the as-received geological specimen *U_0_25*. The rearranged sequence of the diffraction peaks can be seen by the indices listed at the top of the figure.

B. Transmission electron microscopy observations

Galena is a soft though brittle crystal: cleavage along the {100} planes as well as plastic deformation, in the ⟨110⟩{001} slip system, can be induced at relatively low stresses. This is at the origin of many characteristic features of the microstructure of ground PbS geological powders, which can be compared with those observed in ancient cosmetics. So far, we have examined the behavior of two geological galena powders prepared in the laboratory: *U_0_25* (gentle hand-grinding and sieving through a 63–125 μm mesh) and *U_720_25* (*U_0_25* after 12 h grinding).[53] Preliminary observations show that the coarse galena grains contain a complex network of dislocations; in addition to cleavage, grinding has activated the multiplication and gliding of dislocations within the 63–125 μm particles of galena. Foils prepared from the *U_720_25* powder are difficult to observe because of the strong distortion of the lattice. Only limited volumes are adequate to detect the dislocations with a thin contrast. However, estimations of the dislocation densities have been made in various micrographs. They give a factor of 10 between densities induced in coarse and fine particles. This value is in agreement with the x-ray diffraction data (Table II). A more detailed TEM study of the microstructure of galena will be published elsewhere.[53]

C. Effects of crushing and sieving on the microstructure of galena

The volume average crystallite diameter $\langle X\rangle_{\rm vol}$ and the average dislocation density ρ of the nonannealed geological specimens *U*, *E*, and *F* are shown as a function of the ball milling duration t. The crystallite size distribution becomes narrower and is shifted towards the small values with milling period. The size distribution is assumed to be log-normal and is determined by the m and σ values in Tables II and III. The asymmetry of the distribution towards smaller sizes causes a large difference between $\langle x\rangle_{\rm vol}$ and m. In Fig. 4. It can be seen that $\langle X\rangle_{\rm vol}$ decreases strongly with t. $\langle X\rangle_{\rm vol}$ decreases by a factor ~3 within one hour of milling. Comparing the evolution of $\langle X\rangle_{\rm vol}$ and ρ in Figs. 4(a) and 4(b), it can be seen

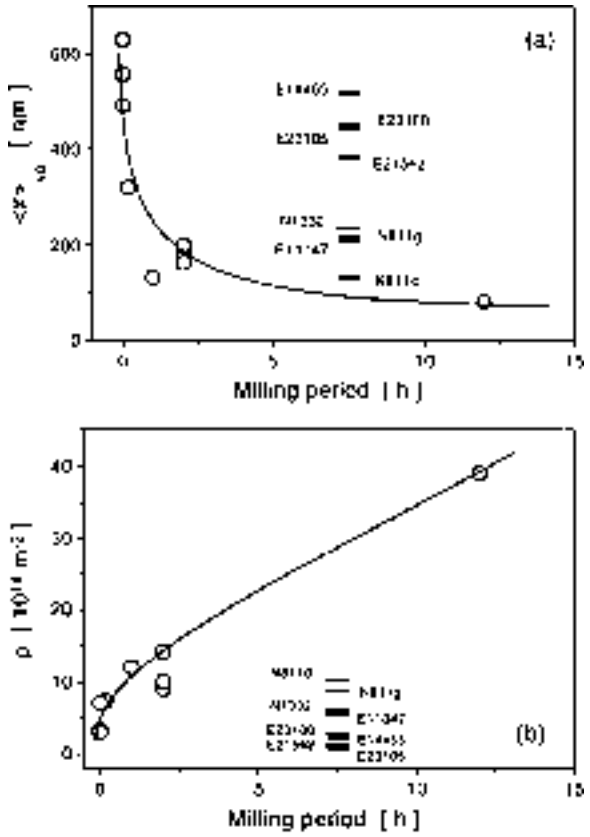

FIG. 4. (a) The volume averaged crystallite diameter $\langle X \rangle_{\mathrm{vol}}$ according to Eq. (5) and (b) the average dislocation density ρ vs (b) the milling time for the geological galena specimens originating from different mining sources. The solid ticks correspond to the values of $\langle X \rangle_{\mathrm{vol}}$ and ρ for the archeological samples.

that with prolonged crushing ρ increases more notably than the crystallite size decreases. The values for *U*, *E*, and *F* specimens are comparable within the error bars, even though the minerals come from very different geological sources. As a result of the initial 63–125 μm mesh sieving, the powder is split into two different populations: *U_0_25* and *Ufin*, whose features (m and σ) are given in Table II. The population of small (<10 μm) crystallites is absent in the size distribution of the sieved powder *U_10_25*. *Ufin* (the fine-grained complementary fraction of *U_10_25* after filtering) has a similar size distribution to the one observed after 10 min crushing (specimen *U_0_25*). *Ufin* and *U_10_25*, whose size distributions are fairly similar, can be separated, though, since their respective ρ values differ by a factor of 2. The SEM images of both powders are similar, and cannot be used for identification of the relevant treatment (sieving or crushing). Therefore these values of $\langle X \rangle_{\mathrm{vol}}$ and ρ, and their respective size distributions, are used as a fingerprint for assessing the manufacturing history of the archæological samples from their microstructure.

D. Effects of annealing on the microstructure of galena

The variation of the average dislocation density ρ as a function of the annealing temperature T (2 h in vacuum), after different periods of milling time t is shown in Fig. 5. for

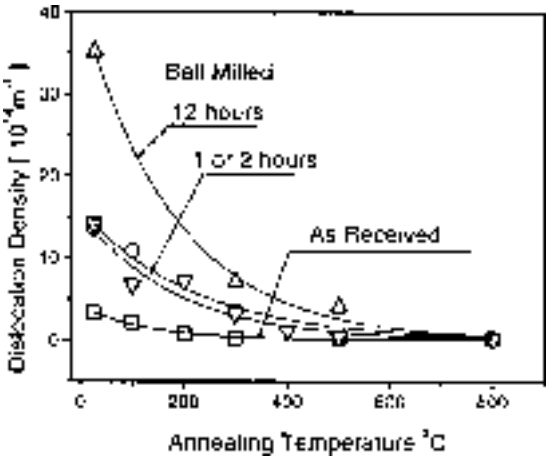

FIG. 5. The average dislocation density ρ as a function of the annealing temperature T (2 h in vacuum), after different periods of milling time t. The solid lines are only guidelines for the eye.

the geological *U* specimens. The dislocation density decreases continuously with increasing annealing temperature, even below 300 °C. ρ does not vary much above 600 °C. By analogy with the behavior of plastically deformed metals,[54] Fig. 5 may be interpreted as: (i) the recovery of microstructural defects by atomic diffusion below 300 °C, (ii) the primary recrystallization of grains, provided T does not exceed ~40% of the melting temperature (1385 K), and (iii) the grain growth, where some grains coalesce as a result of boundary diffusion at higher temperatures. We may compare the effect of 2 h annealing at 100 °C and 300 °C on the site distribution functions of galena after 1 h mechanical grinding: *U*_60_25, *U*_60_100, and *U*_60_300. It can be been that annealing at 100 °C leaves the site distribution practically unchanged, whereas annealing at 300 °C increases the mean crystallite size and shifts the size distribution. It broadens and becomes more symmetric on annealing, i.e., the ratio of $\langle x \rangle_{\mathrm{vol}}$ over the median m decreases.

V. ARCHÆOLOGICAL INTERPRETATION OF THE MICROSTRUCTURE OF GALENA IN EGYPTIAN MAKEUP

We did not find any ancient document which could suggest that heating was part of the preparation procedure. Therefore heating will only be considered in very few archæological cases, whenever the observation of the crystallite microstructure and habit and the existence of the oxidized PbS phase support that assumption. The correlation between the archæological and geological specimens is established in two steps. First, the closest nonannealed geological states to each archæological sample are selected, considering the dislocation density ρ and the volume average crystallite size $\langle X \rangle_{\mathrm{vol}}$ in Fig. 4. In a second step, an attempt is made to identify the best correspondence using the size distribution functions. In the first step, Fig. 4 suggests the archæological specimens be sorted into two groups.

Group(I): $N811d$, $N811g$, $N1332$, and $E11047$

Group(II): $E23100$, $E14455$, $E21562$, and $E23105$

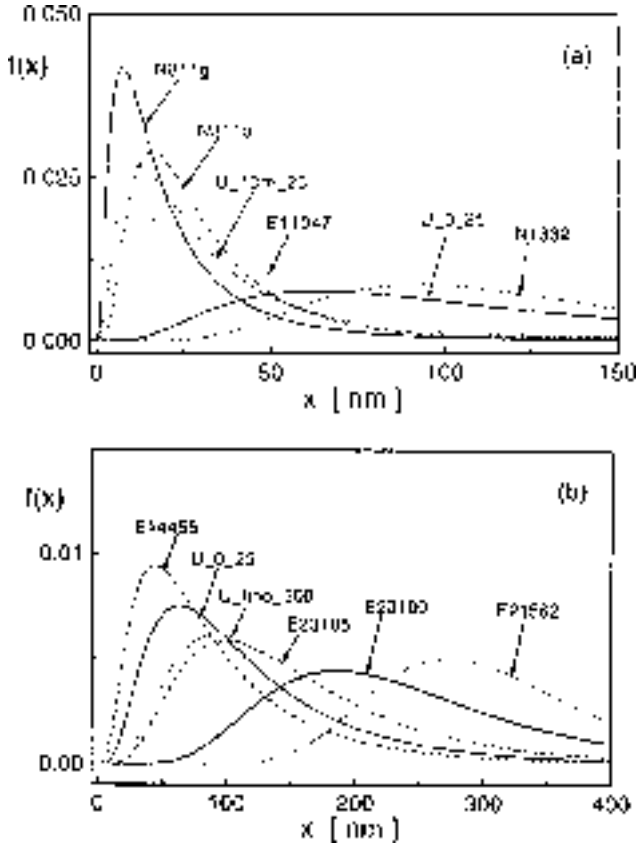

FIG. 6. The crystallite size distributions $f(x)$ of all archeological specimens constructed by using the m and σ values (see Table III) and Eq. (3). (a) Group I (see Sec. V) together with *U_0_25* and *U_10_25* and (b) Group II (see Sec. V) together with *U_0_25* and *Ufin_300* (the fine fraction of the as-received galena annealed at 300 °C for 2 h).

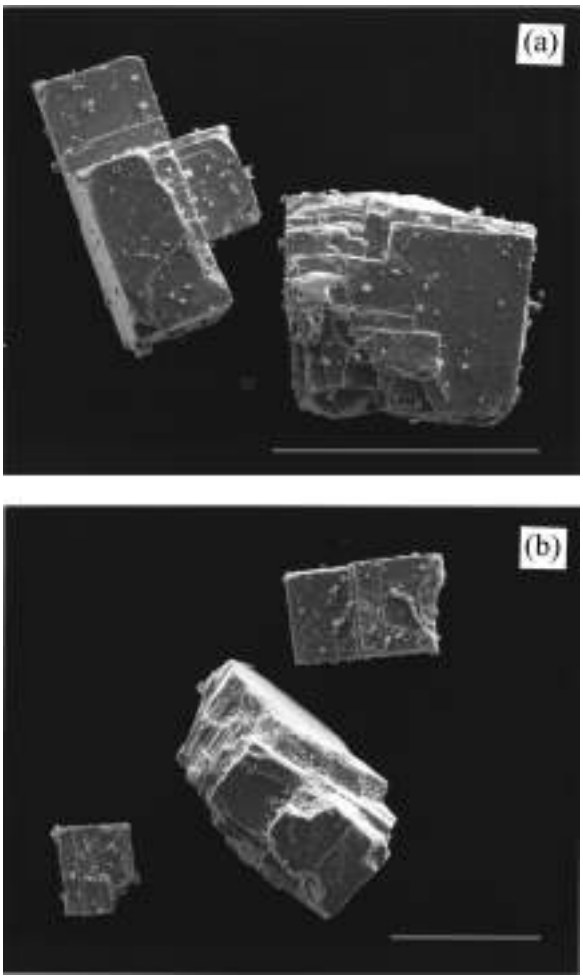

FIG. 7. SEM micrographs of the specimens: (a) *U_0_25* and (b) *E*23105 The horizontal white lines in the lower right corners are 100 μm.

A. Group I

The dislocation densities ρ of the archæological specimens *E11047*, *N1332*, *N811g*, and *N811d* are relatively high, between 5×10^{14} and $10\times10^{14}\,\mathrm{m}^{-2}$ (Table III). The volume average crystallite sizes $\langle X\rangle_{\mathrm{vol}}$ are relatively small, between 130–240 nm. Both parameters strongly suggest that these archæological powders were ground (high ρ and small $\langle X\rangle_{\mathrm{vol}}$). All the size distributions but one (*N1332*) are close to the size distributions of the geological specimens *U_10_25* and *U_60_25*, and markedly different from that of *U_0_259* [Fig. 6(a)]. Therefore, by comparison with the geological simulations, we believe these powders were crushed, the equivalent of ~10 min to 1 h grinding in an automatic device. The large contrast between m and $\langle X\rangle_{\mathrm{vol}}$ shows that the distribution is asymmetric, i.e., the proportion of small particles largely dominates in these populations of grains. All three (*E11047*, *N811g*, and *N811d*) consist of a fine-grained powder. After crushing, we think that these powders were possibly sieved or decanted: consequently, the largest particles were removed, and one was left with a homogeneous dustlike powder made of fine particles with a black mat texture. Concerning *N1332*, the values of ρ, and $\langle X\rangle_{\mathrm{vol}}$ are similar to those in the former specimens, but the size distribution [Fig. 6(a)] is shifted rightwise, and the $\langle X\rangle_{\mathrm{vol}}$-to-$m$ ratio is smaller. That suggests the presence of bigger crystallites, i.e., the grains in the crushed specimen *N1332* were not as well separated out. Optical microscopy observations indicate that the powder contains large, shiny grains dispersed among the finer fraction of the powder.

B. Group II

All the specimens of this group lie in an interval of larger crystallite sizes $\langle X\rangle_{\mathrm{vol}}$, between 400 and 550 nm; the average dislocation density ρ is lower, between 1×10^{14} and $3\times10^{14}\,\mathrm{m}^{-2}$ (see Table III). The size distribution of *E23105* is rather broad [Fig. 6(b)], and very similar to that of sample *U_0_25*. The SEM micrographs in Figs. 7(a) and 7(b) of samples *U_0_25* and *E23105* show that the crystal habit and the powder granulometry are very similar. The galena grains consist of small cubes with cleaved faces and homogeneous dimensions between 20 and 100 μm. The dustlike fraction of finer particles is not observable. On this basis, we assume that galena in *E23105* was gently crushed and sorted out by sieving for larger grain size. This soft treatment, as applied to our reference specimen *U_0_25*, produces a bright-looking powder of loose texture, consisting of shiny-gray, high-reflectivity crystallites. This practice of sieving the galena was described at a later period by Pliny the Elder: ''galena is crushed and then filtered through three layers of tissue.'' [8]

Specimen *E*14455 exhibits a distribution intermediate between *U_0_25* and *Ufin*; the contrast between $\langle X\rangle_{\mathrm{vol}}$ and *m* is larger than in *E*23105. Therefore the peak profile analysis of *E*14455 suggests a rather heterogeneous powder, containing a mixture of small and large particles with no clear trace of crushing. *E*14455 does not seem to have been transformed significantly once extracted from its parent ore. Although samples *E*23100 and *E*21562 show similar $\langle X\rangle_{\mathrm{vol}}$ and ρ parameters, their particle size distributions in Fig. 6(b) differ significantly from those of *E*14455 and *E*23105: the distributions are shifted towards higher values, and are more Gaussian-like (small $\langle X\rangle_{\mathrm{vol}}$-over-*m* ratio). These features were previously mentioned as a consequence of annealing. As a matter of fact, both the archæological specimen *E*23100 and the geological specimen *U_0_200* exhibit very similar size distributions. In addition, samples *E*23100 and *E*21562, respectively, contain about 20% and 10% of anglesite ($PbSO_4$).[55] This oxide could have been formed by oxidation of galena under heating in air. Since $PbSO_4$ decomposes into lanarkite above 400 °C,[56] whose presence could not be detected in either *E*23100 or *E*21562, the annealing temperature was probably lower than 400 °C. There is no evidence of any cooking of galena in Ancient Egypt, although a contemporary North African recipe mentions that ''galena should be wrapped in a piece of thick blue blanket and be left over a coal heater and covered up with ash.''[57] On heating, one observes that the oxide layer formed over the surface of the PbS grains induces some yellow tones, and turns blue above 400 °C.[56] This coloring effect, if desired during the preparation of the makeup, could not be confirmed in the archæological specimens since the volumes of the sampled powders were too small. Because sample *E*21562 also contains 20% mass of laurionite (PbOHCl), which decomposes above 160 °C, it is likely that the galena was heated up before being incorporated into the mixture. From the joint analysis of the microstructure and the complementary phase analysis, we conclude that *E*23100 and *E*21562 were probably crushed more severely than *E*14455 and *E*23105, and subsequently heated to relatively high temperatures, between 200 and 300 °C.

Note that the examination of the SEM micrographs is insufficient in a number of cases. The complementary peak profile analysis of diffraction data has the advantage of giving some quantitative information. For example, *N*1332 and *E*14455 have different microstructure parameters, although their respective SEM images are very similar, *N*1332 was presumably more severely crushed (larger ρ and smaller $\langle X\rangle_{\mathrm{vol}}$). In another example, specimens *E*11047, *N*811*g*, and *N*811*d* as well as *Ufin* contain conglomerates of small grains; the powders in *E*11047, *N*811*g*, and *N*811*d* all probably resulted from a filtering process as *Ufin* does. However, the large residual density of defects measured in the archæological crystallites is the signature of some stress previously applied (probably to reduce and fragment most of the galena blocks into small grains, with no or little loss of matter). On the contrary, a lower density of defects is measured in the small grains of *Ufin*, because they were directly obtained by sieving the geological powder *U_0_25*. In a third example, one can discriminate a raw or moderately crushed powder (e.g., *E*14455) from a crushed and annealed powder (e.g., *E*23100 and *E*21562) by (i) the shape of the respective size distributions and (ii) the presence/absence of oxidized galena. In that particular case, the identification of the present phases by diffraction is also a useful element.

In summary, the microstructure of the archæological specimens as determined in the present work, supported by complementary SEM, TEM and qualitative/quantitative phase analysis, suggests the following manufacturing procedures of ancient Egyptian makeups:

1) gentle crushing:	*E*14455
2) gentle crushing and sieving:	*E*23105
3) crushing:	*N*1332
4) crushing and sieving:	*E*11047, *N*811*d*, and *N*811*g*
5) crushing and heating (200–300 °C):	*E*23100 and *E*21562.

VI. CONCLUSION

The average microstructure of the main ore ingredient (galena) has been identified in several black eye makeups in ancient Egypt, using high-resolution x-ray diffraction data. The modeling method implemented in the present work enabled us to derive, in particular, the dislocation densities ρ, the volume averaged diameters $\langle x\rangle_{\mathrm{vol}}$, and the size distribution of the archæological galena crystallites. The dislocation density, crystallite size, and size distributions are used as fingerprints and compared with the values of artificially crushed and annealed geological PbS samples. Hence these microstructure parameters help in the interpretation of the manufacturing procedures applied by ancient Egyptians to produce eye makeups based on PbS powders (galena).

The Fourier coefficients of the individual observed diffraction profiles of geological and archæological galena were fitted by the Fourier coefficients of physical functions of size and strain profiles. The size profiles were determined by assuming spherical crystallites with a log-normal size distribution, and are characterized by the median *m* and the variance σ of the size distribution function. The Fourier coefficients of the strain profiles were taken from Wilkens[14] in the entire relevant *L* range, assuming that strain is caused by dislocations. The entire strain profile is characterized by two parameters: the dislocation density ρ and the effective outer cutoff radius R_e. The *hkl*-dependent strain-broadening contribution into each overall diffraction profile has been accounted for by the *hkl*-dependent average dislocation contrast factors defined by a single parameter *q*.

Four or five different types of technological procedures could be identified. The discussion of the microstructure is further supported by the direct morphological description provided by SEM and TEM micrographs, some qualitative and quantitative phase analysis results, and auxiliary archæological information. It is established that the color of the black powder could be controlled by mixing together the black ore (galena) and the white ore (cerussite $PbCO_3$).[8,9] In the present work we show that the granulometry, the texture, and the surface state of galena in the makeup can be controlled by milling/sieving/annealing. In some instances

crushing the powder into a dispersed dust could have been deliberate in order to increase the adherence, the contact, and the reaction area with the skin. This particular conditioning of the powder, and the presence of two more white lead synthetic ingredients, laurionite PbOHCl and phosgenite $Pb_2Cl_2CO_3$, might have conferred some medical function to the powder and were appropriate for body care.

ACKNOWLEDGMENTS

T.U. and G.R. are grateful for the financial support of the Hungarian Scientific Research Fund, OTKA, Grant Nos. T031786, T034666, and T029701. The archæological objects from the Department of the Egyptian Antiquities of Le Louvre Museum have been kindly handed over by C. Ziegler and G. Pierrat. This work is part of the research program on the ''practices and use of cosmetics in Antiquity,'' supported by the Center National de la Recherche Scientifique and L'Oréal-Recherche.

[1] R. J. Forbes, in *Studies in Ancient Technology*, edited by E. J. Brill (Leiden, 1955) Vol. III, pp. 1–49.
[2] A. Lucas and J. R. Harris, in *Ancient Egyptian Materials and Industries*, (Edward Arnold, London, 1962) p. 523.
[3] F. Jonckheere, Historie de la Médecine, **7**, 2 (1952).
[4] L. Troy, Bull. d'Egyptologie, **106/1**, 351 (1993).
[5] Z. El-Kordy, in *Annales du Service des Antiquités de l'Egypte*, (1982), Vol. LXVIII, p. 195.
[6] J. Vandier d'Abbadie, in *Catalogue des Objets de Toilette Égyptiens du Musée du Louvre* (Réunion des Musées Nationaux, Paris, 1972), p. 191.
[7] Ph. Walter, P. Martinetto, G. Tsoucaris, R. Bréniaux, M.-A. Lefebvre, G. Richard, J. Talabot, E. Dooryhée, Nature (London) **397**, 483 (1999).
[8] H. Zehnacker, in *Pline l'Ancien, Histoire Naturelle*, (Les Belles Lettres, Paris, 1983) Vol. XXXIII, p. 252.
[9] M. Wellman, in *Dioscoridis Pedanii, De Materia Medica, Libri Quinque* (Weidmannsche Verlagsbuchhandlung, Vienna, 1958).
[10] T. Bardinet, in *Les papyrus médicaux de l'Egypte pharaonique* (Fayard, Paris, 1995), p. 591.
[11] A. Guinier, in *X-ray Diffraction* (Freeman, San Francisco, 1963).
[12] J. I. Langford, D. Louër, and P. Scardi, J. Appl. Crystallogr. **33**, 964 (2000).
[13] T. Ungár, J. Gubicza, G. Ribárik, and T. W. Zerda, in *Proceedings of the MRS Symposium: Filled and Nanocomposite Polymer Materials*, edited by R. P. Hjelm, A. I. Nakatani, M. Gerspacher, and R. Krishnamoorti (MRS, Boston, 2000) pp. KK9.2.1–6.
[14] M. Wilkens, in *Fundamental Aspects of Dislocation Theory*, edited by J. A. Simmons, R. de Wit, R. Bullough (Natl. Bur. Stand. U.S. Spec. Publ. No. 317, Washington, D.C. 1970) Vol. II, p. 1195.
[15] T. Ungár, J. Gubicza, G. Ribárik, and A. Borbély, J. Appl. Crystallogr. **34**, 298 (2001).
[16] G. Ribárik, T. Ungár, and J. Gubicza, J. Appl. Crystallogr. **34**, 669 (2001).
[17] G. K. Williamson and W. H. Hall, Acta Metall. **1**, 22 (1953).
[18] B. E. Warren and B. L. Averbach, J. Appl. Phys. **21**, 595 (1950); **23**, 497 (1952).
[19] B. E. Warren, Prog. Met. Phys. **8**, 147 (1959).
[20] T. Ungár and A. Borbély, Appl. Phys. Lett. **69**, 3173 (1996).
[21] T. Ungár and G. Tichy, Phys. Status Solidi A **171**, 425 (1999).
[22] M. A. Krivoglaz, in *Theory of X-ray and Thermal Neutron Scattering by real Crystals* (Plenum, New York, 1969); and in *X-ray and Neutron Diffraction in Nonideal Crystals* (Springer, Berlin, 1996).
[23] T. Ungár, S. Ott, P. G. Sanders, A. Borbély, and J. R. Weertman, Acta Mater. **10**, 3693 (1998).
[24] T. Ungár, M. Victoria, P. Marmy, P. Hanák, and G. Szenes, J. Nucl. Mater. **276**, 278 (2000).
[25] R. W. Cheary, E. Dooryhée, P. Lynch, N. Armstrong, and S. Dligatch, J. Appl. Crystallogr. **33**, 1271 (2000).
[26] T. Ungár, A. Borbély, G. R. Goren-Muginstein, S. Berger, and A. R. Rosen, Nanostruct. Mater. **11**, 103 (1999).
[27] T. Ungár, M. Leoni, and P. Scardi, J. Appl. Crystallogr. **32**, 290 (1999).
[28] T. Ungár, I. C. Dragomir, D. Louër, and N. Audebrand, J. Phys. Chem. Solids (in press).
[29] G. Ziegler, J. Heinrich, and G. Wötting, J. Mater. Sci. **22**, 3041 (1987).
[30] C. E. Krill and R. Birringer, Philos. Mag. A **77**, 621 (1998).
[31] W. C. Hinds, in *Aerosol Technology: Properties, Behavior and Measurement of Airbone Particles* (Wiley, New York, 1982).
[32] P. Scardi and M. Leoni, J. Appl. Crystallogr. **32**, 671 (1999).
[33] H. Trinkaus, Phys. Status Solidi B **51**, 307 (1972).
[34] I. Gaál, J. Appl. Crystallogr. **8**, 127 (1975).
[35] I. Groma, T. Ungár, and M. Wilkens, J. Appl. Crystallogr. **21**, 47 (1988).
[36] L. E. Levine and R. Thomson, Acta Crystallogr., Sect. A: Found. Crystallogr. **53**, 590 (1997).
[37] I. Groma, Phys. Rev. B **57**, 7535 (1998).
[38] J. D. Kamminga and R. Delhez, J. Appl. Crystallogr. **33**, 1122 (2000).
[39] P. Suortti, in *IUCr Monographs on Crystallography*, edited by R. A. Young (Oxford University Press, New York, 1993) Vol. 5, pp. 167–185.
[40] M. Latroche, J. Rodriguez-Carvajal, A. Percheron-Guéan, and J. Boureé -Vigneron, Alloys & Compounds **218**, 64 (1995).
[41] J. E. Fischer, G. Bendele, R. Dinnebier, P. W. Stephens, C. L. Lin, N. Bykovetz, and Q. Zhu, J. Phys. Chem. Solids **56**, 1445 (1995).
[42] F. W. Gayle and F. S. Biancaniello, Nanostruct. Mater. **6**, 429 (1995).
[43] P. W. Stephens, J. Appl. Crystallogr. **32**, 281 (1999).
[44] N. C. Popa, J. Appl. Crystallogr. **33**, 103 (2000).
[45] T. Ungár, I. Dragomir, Á. Révész, and A. Borbély, J. Appl. Crystallogr. **32**, 992 (1999).
[46] S. Kim and H. Ledbetter, J. Appl. Phys. (submitted).
[47] C. I. Dragomir and T. Ungár, J. Phys. Chem. Solids. (submitted).
[48] P. Martinetto, M. Anne, E. Dooryhée, and P. Walter, J. Phys. IV **10**, 465 (2000).
[49] A. N. Fitch, Mater. Sci. Forum **228–231**, 219 (1996).
[50] G. Courbion and G. Férey, J. Solid State Chem. **76**, 426 (1988).
[51] O. Masson, E. Dooryhée, R. W. Cheary, and A. N. Fitch, Mater. Sci. Forum (Proceedings EPDIC Barcelona, 2000) (in press).
[52] A. R. Stokes, Proc. Phys. Soc. London **61**, 382 (1948).
[53] P. Martinetto, J. Castaing, P. Penhoud, P. Veyssière, and P. Walter, J. Mater. Res. (submitted for publication).
[54] Y. Adda, J. M. Dupouy, and J. Philibert, and Y. Quéré, in *Eléments de métallugie physique, Déformation plastique 5* (CEA-INSTN, Saclay, France, 1991).
[55] P. Martinetto, Ph.D. Thesis, Université de Grenoble, 2000.
[56] B. Ponsot, J. Salomon, and P. Walter, Nucl. Instrum. Methods Phys. Res. B **136–138**, 1074 (1988).
[57] A. Dairi, Ph.D. Thesis, Université de Nancy, 1991.